



CCL2: a Chemokine Potentially Promoting Early Seeding of the Latent HIV Reservoir

Thomas A. Packard,^{a,*} Roland Schwarzer,^{a,b} Eytan Herzig,^{a,§} Deepashri Rao,^c Xiaoyu Luo,^a Johanne H. Egedal,^{a,◇} Feng Hsiao,^a Marek Widera,^d Judd F. Hultquist,^{a,e,i,∞} Zachary W. Grimmer,^a Ronald J. Messer,^c Nevan J. Krogan,^{a,e,i} Steven G. Deeks,^f Nadia R. Roan,^{a,g} Ulf Dittmer,^{b,d}  Kim J. Hasenkrug,^c  Warner C. Greene^{a,f,h}

^aJ. David Gladstone Institutes, San Francisco, California, USA

^bInstitute for Translational HIV Research, University Hospital Essen, University of Duisburg-Essen, Essen, Germany

^cLaboratory of Persistent Viral Diseases, Rocky Mountain Laboratories, National Institute of Allergy and Infectious Diseases, National Institutes of Health, Hamilton, Montana, USA

^dInstitute for Virology, University Hospital Essen, University of Duisburg-Essen, Essen, Germany

^eQuantitative Biosciences Institute (QBI), University of California San Francisco, San Francisco, California, USA

^fDepartment of Medicine, University of California San Francisco, San Francisco, California, USA

^gDepartment of Urology, University of California San Francisco, San Francisco, California, USA

^hDepartment of Microbiology and Immunology, University of California San Francisco, San Francisco, California, USA

ⁱDepartment of Cellular and Molecular Pharmacology, University of California San Francisco, San Francisco, California, USA

Thomas A. Packard and Roland Schwarzer contributed equally to this work. Author order was determined in order of increasing seniority.

ABSTRACT HIV infects long-lived CD4 memory T cells, establishing a latent viral reservoir that necessitates lifelong antiretroviral therapy (ART). How this reservoir is formed so quickly after infection remains unclear. We now show the innate inflammatory response to HIV infection results in CCL2 chemokine release, leading to recruitment of cells expressing the CCR2 receptor, including a subset of central memory CD4 T cells. Supporting a role for the CCL2/CCR2 axis in rapid reservoir formation, we find (i) treatment of humanized mice with anti-CCL2 antibodies during early HIV infection decreases reservoir seeding and preserves CCR2/5⁺ cells and (ii) CCR2/5⁺ cells from the blood of HIV-infected individuals on long-term ART contain significantly more integrated provirus than CCR2/5-negative memory or naive cells. Together, these studies support a model where the host's innate inflammatory response to HIV infection, including CCL2 production, leads to the recruitment of CCR2/5⁺ central memory CD4 T cells to zones of virus-associated inflammation, likely contributing to rapid formation of the latent HIV reservoir.

IMPORTANCE There are currently over 35 million people living with HIV worldwide, and we still have no vaccine or scalable cure. One of the difficulties with HIV is its ability to rapidly establish a viral reservoir in lymphoid tissues that allows it to elude antivirals and the immune system. Thus, it is important to understand how HIV accomplishes this so we can develop preventive strategies. Our current results show that an early inflammatory response to HIV infection includes production of the chemokine CCL2, which recruits a unique subset of CCR2/5⁺ CD4⁺ T cells that become infected and form a significant reservoir for latent infection. Furthermore, we show that blockade of CCL2 in humanized mice significantly reduces persistent HIV infection. This information is relevant to the development of therapeutics to prevent and/or treat chronic HIV infections.

KEYWORDS CCL2, CRISPR, CyTOF, human immunodeficiency virus, latency, reservoir

The latent HIV reservoir is comprised of both fully infectious and defective proviruses residing predominantly within memory CD4 T cells. These cells are not effectively depleted by antiretroviral therapy (ART); thus, lifelong treatment is required to

Editor Anne Moscona, Columbia University Medical College

This is a work of the U.S. Government and is not subject to copyright protection in the United States. Foreign copyrights may apply.

Address correspondence to Warner C. Greene, warner.greene@gladstone.ucsf.edu.

*Present address: Thomas A. Packard, Shape Therapeutics, Seattle, Washington, USA.

§Present address: Eytan Herzig, Chimeria Bioengineering, San Francisco, California, USA.

◇Present address: Johanne H. Egedal, Regionshospitalet Horsens, Horsens, Aarhus, Denmark.

∞Present address: Judd F. Hultquist, Department of Medicine, Division of Infectious Diseases, Northwestern University Feinberg School of Medicine, Chicago, Illinois, USA.

The authors declare no conflict of interest.

This article is a direct contribution from Ulf Dittmer, a Fellow of the American Academy of Microbiology, who arranged for and secured reviews by George Lewis, Institute of Human Virology, University of Maryland School of Medicine, and Leonid Margolis, NIH/NICHD.

Received 4 August 2022

Accepted 16 August 2022

Published 8 September 2022

prevent disease progression. In rhesus macaques, a stable SIV reservoir is established within 3 days or less following infection (1). Likewise, the HIV reservoir is rapidly seeded in humans (2–4). Recently, it has been demonstrated that ART modulates and shapes the host environment in a way that favors long-term survival of the cells and viral quasispecies that predominate at the time of treatment initiation (5, 6). This phenomenon is likely reflective of a continuous reservoir seeding throughout the time prior to ART (7), which is characterized by chronic inflammation and immune activation (8).

HIV preferentially infects effector CD4 T cells (9, 10), but because these cells are terminally differentiated and short-lived, they do not contribute to formation of a long-lived latent reservoir. In contrast, infection of memory CD4 T cells is required, but the underlying mechanisms for such infections remain unknown (11–14).

Chemoattraction might play an important role. Acute HIV infection leads to the production of many cytokines and chemokines. Prominent among these is the C-C motif ligand 2 chemokine (CCL2/monocyte chemoattractant protein 1 [MCP-1]) (15–17). CCL2 is one of the first cytokines detected during the acute phase of HIV infection, preceding peak viremia and correlating with viral load (15, 16, 18). CCL2's swift upregulation during acute infection raises the possibility that it helps recruit cells involved in latent reservoir formation.

In these studies, we set out to explore the CCL2-CCR2 chemokine/chemokine receptor axis during acute HIV infection, asking whether it might play a positive role in early formation of the latent viral reservoir through recruitment of central memory CD4 T cells to tissue sites of infection and inflammation.

RESULTS

HIV triggers IFI16/STING signaling to produce CCL2 in lymphoid CD4 T cells. To investigate whether CCL2 is induced in lymphoid tissue-derived CD4 T cells in response to HIV, we used a previously described *in vitro* cell overlay model employing human tonsillar cells (19). This method allows for the rapid, synchronous infection of CD4 T cells. When measured 18 h after infection, transcription of CCL2 and IFNB1 was significantly upregulated while transcription of CCL20, an alternative STAT6-regulated chemokine, was not induced (Fig. 1A; also see Fig. S1A in the supplemental material). CCL2 protein levels were also increased in the supernatant measured at 24 h after infection (Fig. 1B). In prior studies, blood-derived CD4 T cells were found to poorly induce innate immune responses to HIV (19–21). Indeed, in contrast to lymphoid tissue CD4 T cells, blood CD4 T cells failed to produce CCL2 (Fig. S1B). Basal levels of CCL2 expression were also higher in uninfected CD4 T cells from lymphoid tissue than in those from blood, underscoring the importance of studying tissue-derived T cells in models of HIV infection.

To assess whether successful viral integration and HIV replication were required for the induction of CCL2 synthesis, we added the integrase inhibitor raltegravir during overlay infection and assessed CCL2 release from infected cells (Fig. S1B). CCL2 production was unaffected by raltegravir treatment, indicating the preintegration steps of the viral life were responsible for the induction of the chemokine. This suggested induction of CCL2 during an abortive infection, in which the accumulation of unintegrated DNA reverse transcripts triggers an inflammatory innate response. This could potentially be triggered by the stimulator of interferon genes STING, which can itself be activated by either one of two DNA sensors: the pyroptosis inducer IFI16 and the cytosolic DNA sensor cyclic GMP-AMP synthase (cGAS). To determine which DNA sensors were driving CCL2 production in lymphoid tissue CD4 T cells, we knocked out the IFI16, STING, or cGAS genes using CRISPR-Cas9 ribonucleoproteins and specific guide RNAs (Fig. 1C). Knockout of either IFI16 or STING resulted in significantly decreased CCL2 release following HIV infection compared to nontargeted controls (Fig. 1D). The decrease in CCL2 release from knocking out cGAS did not reach statistical significance. Together, these results indicated that the innate DNA sensing pathway involving IFI16 and STING and

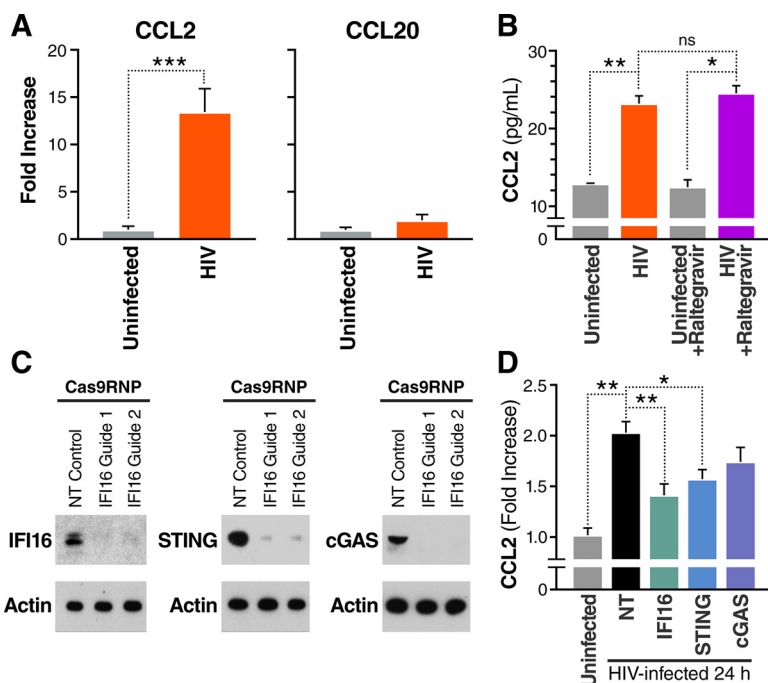


FIG 1 Tonsillar CD4 T cells produce CCL2 following HIV infection in part mediated through IFI16 and STING signaling. Tonsillar CD4 T cells were purified by negative bead selection and infected with HIV (pNL4-3-GFP) by overlay infection as previously described (19). (A) Production of CCL2 and CCL20 RNA was measured by qPCR and plotted as fold increase relative to uninfected controls following 18 h of overlay infection. (B) CCL2 protein secretion measured by Meso Scale Discovery (MSD) was detected following 24 h after HIV infection in overlay cultures employing tonsillar CD4 cells. Addition of raltegravir (an HIV integrase inhibitor) did not block production of CCL2. (C) Cas9 RNPs and two independent guide RNAs were used to knock out IFI16, STING, and cGAS protein expression in primary tonsillar CD4 T cells (NT: nontargeting guide RNA control). (D) CCL2 protein production was significantly diminished (but not eliminated) in HIV-infected cultures when IFI16 or STING was knocked out. Supernatants were harvested 24 h after infection for MSD analysis of CCL2 production. Fold increase over uninfected control is shown for each knockout culture. Experiments were performed with 4 to 6 independent tonsils. Error bars denote SEM; data were analyzed for significance using ANOVA with Tukey's multiple comparisons. *, $P < 0.05$; **, $P < 0.01$; ***, $P < 0.001$; ns, not significant.

possibly cGAS contributed to the rapid synthesis and release of CCL2 by lymphoid CD4 T cells in response to HIV infection.

CCR2 is expressed by a population of CCR5⁺ central memory cells. A major function of CCL2 production is to recruit cells bearing the CCL2 receptor, CCR2 (22, 23). While CCR2 is highly expressed on monocytes, it is also found on a unique subset of blood CCR5⁺ CD4 T cells displaying an effector memory phenotype (24).

We therefore asked whether such CD4 T cells were also present in lymphoid tissue. Indeed, using flow cytometry (Fig. 2A to C), we found that one-third of tonsillar CCR5⁺ cells coexpressed CCR2, compared to two-thirds in the blood (Fig. 2D). To examine more deeply the phenotype of these cells, we compared the expression levels of 38 markers in blood and lymphoid tissue CD4 T cells using mass spectrometry (Fig. 2; Table S1) followed by *t*-distributed stochastic neighbor embedding (tSNE) dimensional reduction visualization. Blood- and lymphoid tissue-derived CD4 T cells differed sharply (Fig. 2E), as did the CCR2/5-expressing CD4 T cells, with tonsil-derived cells displaying elevated expression of CD25 (IL-2R α), CD7, ICOS, and CCR7 (Fig. 2F). CD25 expression is upregulated on activated T cells but also constitutively expressed on regulatory T cells (Tregs), suggesting the possibility of the CCR2/5⁺ cells being Tregs. However, the lymphoid CCR2/5⁺ CD25⁺ cells did not express FoxP3, demonstrate their exhibiting an activated rather than regulatory phenotype (Fig. 2 and Fig. S3). The high expression of CCR7 in the lymphoid CCR2/5⁺ cells suggested that these cells were primarily central memory T cells (25). In contrast, CD127 and CCR6 were elevated in the blood-derived CCR2/5⁺ T cells, indicating an effector memory

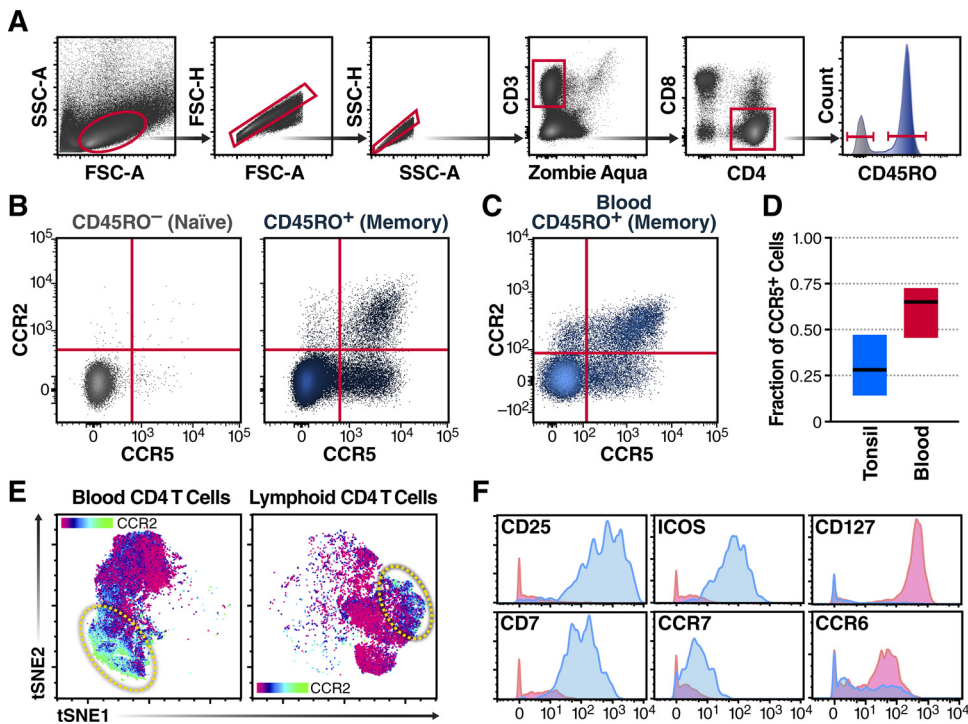


FIG 2 CCR2/5⁺ CD4 T cells in the lymphoid tissue exhibit a distinct phenotype compared to their cellular counterparts circulating in blood. Freshly isolated mononuclear cells from tonsil and blood were analyzed by multicolor flow cytometry. (A) Gating strategy for tonsillar memory CD4 T cells. FSC, forward scatter; SSC, side scatter. (B) CCR2⁺ expression is primarily limited to CCR5⁺ memory T cells in tonsil (gated as in panel A). (C) Representative chemokine receptor expression of blood-derived memory cells. (D) CCR2⁺ is expressed on a significant fraction of CCR5⁺ memory CD4 T cells: 28% ± 11% in tonsil (*n* = 18) and 65% ± 10% in blood (*n* = 8). Box plots show median, 25% quartiles, and maximum and minimum values. (E) Mass cytometry was used to compare blood-derived and lymphoid tissue-derived CD4 cells across 38 different parameters, and tSNE dimensional reduction visualization was performed (*n* = 10 for tonsil and blood). Shown are representative tSNE plots, colored by surface CCR2 expression. (F) Selected markers highlight differences between lymphoid tissue- (blue) and blood-derived (red) CCR2/5⁺ cells. The X-axis shows marker signal indicated in the histograms, Y-axis shows normalized counts. (see Fig. S2 in the supplemental material for further comparisons).

phenotype. Together, these findings underscored fundamental phenotypic differences in lymphoid tissue- versus blood-derived CCR2/5⁺ T cells, highlighting the enrichment of central memory in lymphoid tissues and effector memory in the circulation.

Comparing CCR2/5⁺ lymphoid tissue CD4 T cells to both their naive counterparts and the total memory population shed further light on this unique subset of cells (Fig. 3A). The CCR2/5⁺ cells expressed multiple markers of T cell activation, including surface markers previously shown to be enriched in the latent HIV reservoir. In addition to CD25, these markers included PD1, OX40, and HLA-DR (Fig. 3B) (26–30). Additionally, these CCR2/5⁺ cells expressed ICAM (CD54) and LFA-1a (CD11a), which are important in forming the viral synapse (31). Finally, they expressed a pattern of surface integrins that reflected potential mucosal origins, including integrins alpha 4 and beta 1, as well as alpha-4-beta-7 (32, 33). Taken together, these analyses indicated that lymphoid CCR2/5⁺ cells expressed markers associated with a central memory CD4 T phenotype.

CCR2/5⁺ cells migrate in response to CCL2 and are permissive to HIV infection.

It was previously shown that CCR2/5⁺ CD4 T cells from the blood migrated in response to CCL2 and multiple other chemokines (24). Using a transwell migration assay, we found that lymphoid CCR2/5⁺ cells similarly displayed a chemotactic response to CCL2 (Fig. 4A).

To assess the intrinsic permissiveness of CCR2/5⁺ cells to HIV infection, we sorted fresh tonsillar T cells and exposed them to green fluorescent protein (GFP) reporter viruses expressing either the NL4-3 envelope (X4-tropic) or the BaL envelope (R5-tropic). These cells supported productive infection by both viral strains in the absence

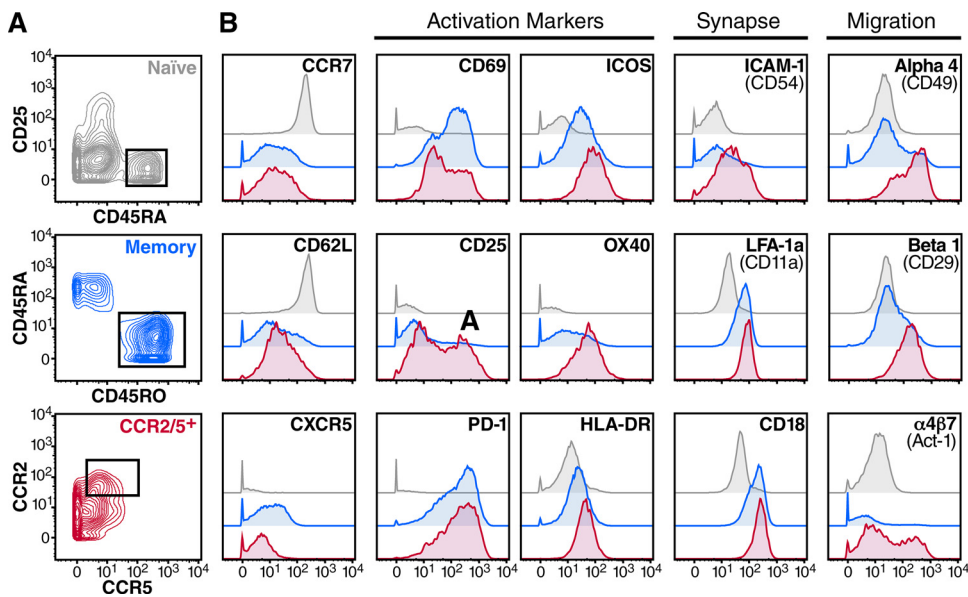


FIG 3 Tonsillar CCR2/5⁺ cells express markers of central memory, activation, viral synapse, and tissue homing. Freshly isolated CD4 T cells from tonsil were analyzed for expression of 38 surface markers by mass cytometry. (A) Gating strategy for naive (pregated on CD3⁺, CD4⁺, CD8⁻, CD45RO⁻ live single cells), memory (pregated on CD3⁺, CD4⁺, CD8⁻ live single cells), and CCR2/5⁺ CD4 T cells (pregated on memory as described above); data shown from representative tonsil ($n = 10$). (B) Comparison of marker expression between populations gated as in panel A (top gray trace, naive; middle blue trace, memory; bottom pink trace, CCR2/5⁺).

of *ex vivo* stimulation (Fig. 4B and C), demonstrating that in their basal state, tonsillar CCR2/5⁺ CD4 T cells were permissive to HIV infection. Interestingly, exogenous CCL2 did not further increase HIV infection of tonsil-derived CD4 T cells (Fig. 4; Fig. S4), although it has been reported to increase the permissiveness of blood T cells to HIV infection (34). These results suggest that the role of CCL2 is primarily in recruitment of CCR2/5⁺ CD4 T cells to the site of HIV infection rather than in increasing their permissiveness to infection.

Of note, exposure to R5-tropic virus induced a rapid loss of surface expression of CCR2 in sorted cells (Fig. 4D), in both infected cells (GFP⁺) and bystander cells (GFP⁻) (Fig. 4D shows all cells, of which GFP⁺ cells are <5%). This effect was not observed following X4-tropic viral infection (Fig. 4D, solid lines). A similar downregulation of CCR5 was observed upon R5-tropic HIV infection. Since this effect was independent of productive infection, it likely reflects internalization of CCR2 and CCR5 triggered by the binding of the viral envelope. It is not currently known whether this downregulation is transient or whether it occurs *in vivo*.

Tonsillar CCR2/5⁺ cells support latent infection by HIV *ex vivo*. Only a fraction of tonsillar CD4 T cells (5 to 10%) undergo productive infection with HIV in the absence of exogenous stimuli. An additional small fraction of cells become latently infected (35, 36). To test whether CCR2/5⁺ cells were able to support latent infection, the cells were sorted as described above and then infected with a luciferase reporter virus in the presence of saquinavir (a viral protease inhibitor) to prevent viral spread. The cells were then allowed to rest in the presence of ART to establish latency, as previously described (36, 37). After 5 days in culture, the cells were stimulated for 24 h with anti-CD3/anti-CD28 antibodies in the presence of the integrase inhibitor raltegravir to ensure measurement of postintegration latency. Luciferase expression was measured as a readout of latent virus reactivation. CCR2/5⁺ cells underwent similar HIV reactivation after stimulation as did CCR2/5⁻ memory cells and significantly greater reactivation than CCR2⁻/5⁺ cells (Fig. 4E). These findings show that HIV can establish a latent and reactivatable form of infection in tonsillar CCR2/5⁺ cells *ex vivo*.

We also measured the survival of CCR2/5⁺ cells following infection with both X4-

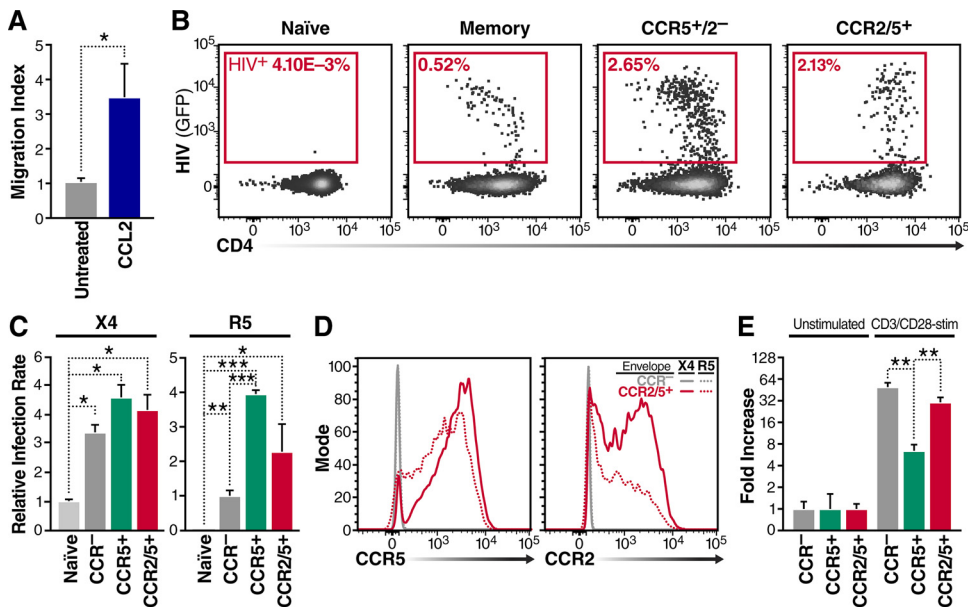


FIG 4 Tonsillar CCR2/5⁺ T cells are permissive to X4- and R5-tropic HIV infection. (A) Transwell migration assay of purified tonsillar CD4 cells added to the upper chamber of a 2- μ m transwell membrane, with 2 ng/mL CCL2 added to the bottom chamber. After 4 h, the migrating cells (collected from the bottom chamber) were analyzed by flow cytometry and counted. Data are presented as a relative migration (fold increase of chemokine receptor-positive over -negative cell migration normalized to untreated control). (B) Assessment of HIV infection in naive, memory (chemokine receptor-negative), CCR5⁺, or CCR2/5⁺ CD4 T cells after sort purification and infection with 100 ng GFP reporter BaL.NL4-3 HIV-1 (R5-tropic). GFP expression denotes productive infection. (C) Relative percentage of GFP-positive cells as gated in panel B, including NL4-3 HIV-1 (X4-tropic) for comparison ($n = 4$). (D) R5-tropic envelope causes loss of surface CCR2. CCR5 and CCR2 levels of sorted CCR-negative memory (gray) or CCR2/5⁺ cells (pink) spinoculated with X4- (solid lines) or R5-tropic (dotted lines) HIV and cultured for 24 h. (E) To assess the ability of tonsillar CCR2/5⁺ cells to support latent infection, a previously described primary CD4 T cell latency model was employed (36). Cells sorted as in panel B were spinoculated with NL4-luciferase reporter virus and cultured in the presence of ART for 5 days. Cells were then reactivated with anti-CD3/28 beads for 24 h. Virus production after reactivation was measured by quantitating luciferase activity. Data are presented as fold increases in stimulated cells relative to unstimulated cells. Experiments involved the analysis of 4 to 8 independent tonsil preparations. Error bars denote SEM by ANOVA with Tukey's multiple comparisons. *, $P < 0.05$; **, $P < 0.01$; ***, $P < 0.001$.

and R5-tropic virus. We found that the fraction that died following infection was quite similar to that of total tonsillar CD4 cells, with approximately two-thirds of cells surviving 48 h after infection (Fig. S5). Together, these results show that HIV infection of CCR2/5⁺ cells can result in multiple outcomes: productive infection, latent infection, or death.

CCL2 blockade reduces seeding of the latent HIV reservoir in humanized mice.

We next tested the role of CCL2 in the establishment of the HIV reservoir *in vivo*, using a bone marrow, liver, thymus (BLT)-humanized mouse model of HIV infection (38) and a CCL2-blocking antibody. At 12 weeks after grafting, all mice were tested for humanization levels, and mice with equivalent human CD4⁺ T cell numbers were placed in the anti-CCL2 ($n = 35$) or control ($n = 34$) antibody groups (Fig. 5A). The mice were infected with the R5-tropic virus JR_{CSF}, previously shown to establish long-term latent HIV infections that persist despite antiretroviral therapy (ART) (38). Intrarectal HIV inoculations were performed daily for 5 days to model sexual transmission via the mucosal route (Fig. 5B). This intrarectal infection protocol was previously shown to produce ~50% infection rates (39). Beginning 24 h prior to the first virus inoculation, the mice were treated with either blocking anti-CCL2 antibody or an isotype control antibody every other day for the first 11 days (Fig. 5B). To evaluate the early establishment of latent infections, HIV replication was disrupted beginning 2 days after the final virus installation (7 days postinfection [dpi]) by placing the mice on ART-infused chow containing tenofovir disoproxil-fumarate (Viread), emtricitabine (Emtriva), and raltegravir (Isentress). Treatment interruption, which was previously shown to reactivate the latent

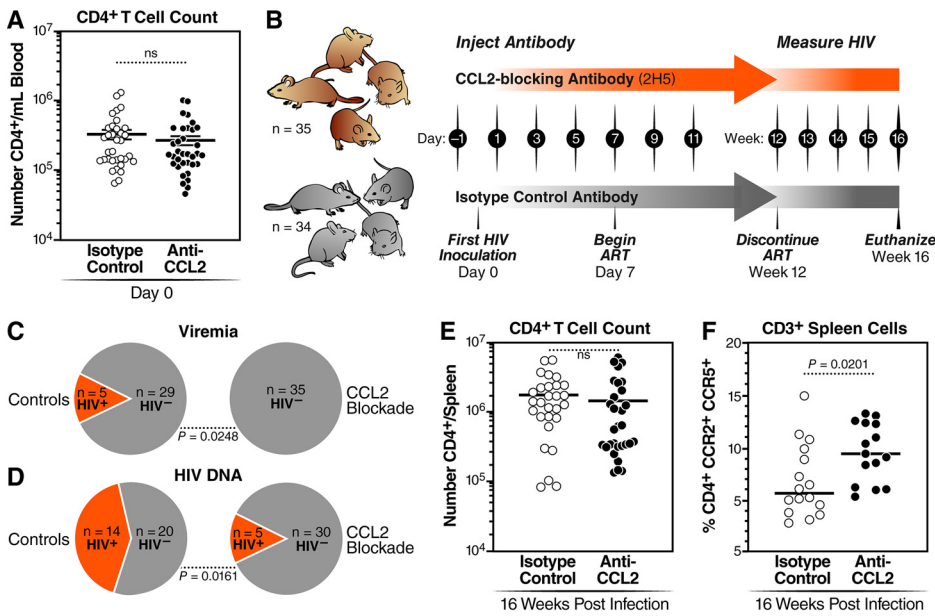


FIG 5 Blockade of CCL2 reduces seeding of the HIV reservoir in humanized mice. (A) BLT mice were humanized as described in the text, and mice with equivalent CD4⁺ T cells at 12 weeks posthumanization were assigned to anti-CCL2 and isotype control groups. (B) Diagram of experimental design illustrating the time course of the experiment. Humanized mice began injections of CCL2-blocking antibody (2H5) or isotype control beginning at 24 h preinfection and every other day thereafter until day 11. Mice were challenged with HIV intrarectally at day 0 and again every 24 h for 5 days. At day 7 the mice were administered ART orally in their chow. ART was maintained for 11 weeks and discontinued at week 12 to begin treatment interruption. Mice were bled weekly following ART interruption and euthanized at week 16 postinfection. (C) Plasma samples were analyzed for HIV RNA by PCR as described in Materials and Methods. Statistical analysis of the contingency table was done by two-sided Fisher’s exact test. (D) Spleen cells were analyzed for both total and integrated HIV DNA levels. Animals that tested positive in either assay were considered positive. Statistical analysis of the contingency table was done by two-sided Fisher’s exact test. (E) The levels of splenic CD4⁺ T cells at 16 wpi were analyzed by flow cytometry and found to be similar in the two groups of mice. (F) Spleen cells were further analyzed for proportions of CCR2/5⁺ in the CD4⁺ subset by flow cytometry. Technical problems occurred in one experiment such that data were not obtained from all the mice. For the remaining mice (*n* = 16 for the controls and *n* = 15 for CCL2 blockade), statistical analysis by two-way Student’s *t* test showed a significant difference between the groups.

HIV reservoir (38–40), was initiated at week 12 by switching the mice to normal chow (Fig. 5B).

At 1 week following treatment interruption (week 13), 3 of 34 isotype control mice were positive for plasma HIV RNA by PCR, and by week 16, when the experiment was terminated, two more tested positive for viremia (Fig. 5C). This low number of mice with reactivated virus in the control group was likely due to the early initiation of ART. None of the 35 animals in the CCL2 blockade group developed detectable viremia during treatment interruption (*P* = 0.0248 by Fisher’s exact test). At week 16, the animals were euthanized, and splenic tissue was harvested and examined for HIV DNA using PCR assays for both total and integrated HIV proviral DNA (41). Data compiled from both assays showed that 14/34 animals (41%) from the isotype control arm had detectable HIV DNA, whereas only 5/35 (14%) from the CCL2 antibody-treated group were positive (Fig. 5C, *P* = 0.0161 by Fisher’s exact test). Two of the control animals that had detectable HIV RNA in their blood at 13 weeks postinfection (wpi) tested negative for HIV DNA in the spleen at 16 wpi. To determine whether CCL2 blockade during HIV exposure had any long-term effect on the CD4⁺ CCR2/5⁺ cell subset, splenic T cells were analyzed by flow cytometry. Although there was no difference in overall numbers of CD4⁺ T cells between the groups (Fig. 5E), there was a significantly higher proportion of CCR2/5⁺ cells in the group of mice that had been treated with CCL2 blockade (Fig. 5F). These results indicated that CCL2 blockade significantly reduced seeding of the latent HIV reservoir and enhanced preservation of CD4⁺ CCR2/5⁺ cells.

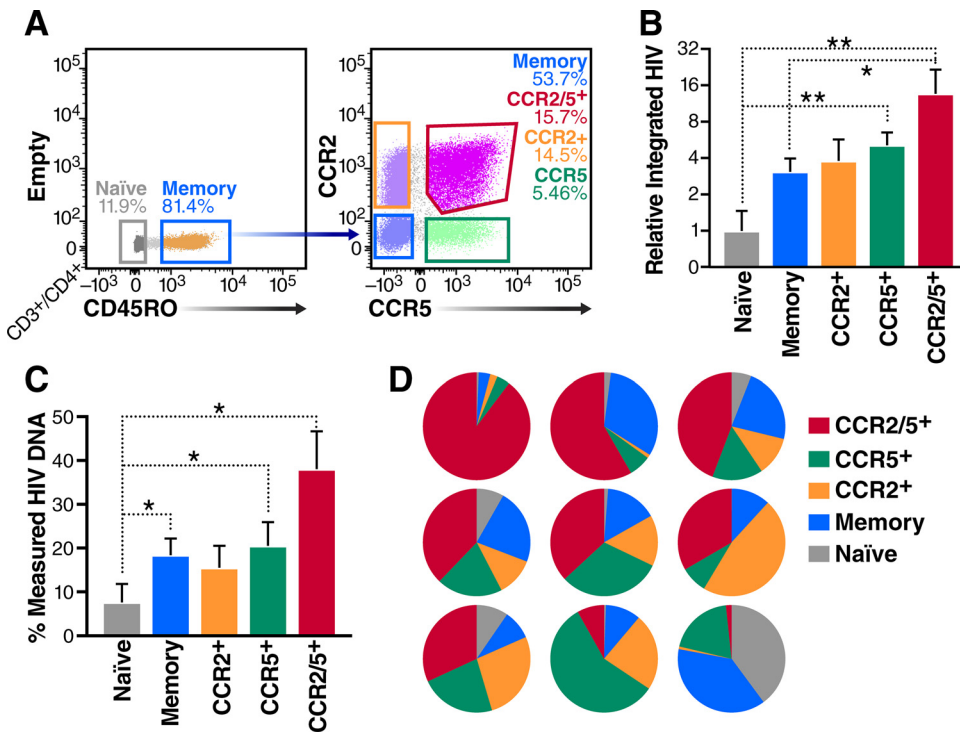


FIG 6 Integrated HIV proviral DNA is enriched in CCR2/5⁺ cells from infected individuals. Naive, memory (CCR⁻), CCR2⁺, CCR5⁺, or CCR2/5⁺ CD4 T cells were purified by cell sorting from leukapheresis samples obtained from ART-suppressed, HIV-infected donors. (A) Example of sorting gates from donor cells, pregated on live, single CD3⁺ CD4⁺ cells. (B) Amount of integrated HIV in sorted cell populations, normalized to mitochondrial DNA and expressed as fold increase over the amount detected in naive cells. Cells were sorted as in panel A, genomic DNA was isolated, and provirus was measured using Alu-Gag droplet digital PCR. (C and D) Distribution of HIV provirus among various cell populations from nine ART-suppressed HIV-infected donors. Results are shown as a percentage of total HIV detected from all subsets for each individual (*n* = 9). Results are grouped by cell type in panel C and separated by individual in panel D. Error bars denote SEM by Friedman ANOVA with Dunn’s test for multiple comparisons. *, *P* < 0.05; **, *P* < 0.01.

CCR2/5⁺ cells harbor HIV provirus *in vivo*. To confirm that CCR2/5⁺ cells played a role in formation of the latent reservoir in ART-suppressed individuals living with HIV, we examined whether CCR2/5⁺ CD4 T cells from such individuals were enriched in HIV proviruses. Fresh leukapheresis samples were obtained from nine ART-suppressed donors from the SCOPE (Observational Study of the Consequences of the Protease Inhibitor Era) cohort at the University of California San Francisco and San Francisco General Hospital (Fig. 6; Table S2). From these samples, CD4 T cells were sorted into naive (CD45RO⁻) and memory (CD45RO⁺) cell populations. The memory population was further separated based on the surface expression of CCR2 and CCR5 (Fig. 6A).

To quantify proviral levels, genomic DNA (gDNA) from sorted cells was isolated and subjected to Alu-Gag droplet digital quantitative PCR (qPCR) to detect integrated HIV provirus. This technique is based on a nested PCR, in which an Alu-Gag amplicon is preamplified and a second internal set of primers plus probe is used to detect HIV. Using this assay, we observed that CCR2/5⁺ cells contained significantly higher levels of integrated HIV than did CCR2/5⁻ memory cells or naive cells (Fig. 6B to D). By comparing the level of HIV DNA in the sorted populations to that in the total population of sorted CD4 T cells, we were able to quantify the percentages of total HIV provirus in each cell population for each donor (Fig. 6C and D). Considerable individual-to-individual differences were observed. One individual exhibited a reservoir that was nearly 90% within the CCR2/5⁺ population, while in others this percentage was lower. The median percentage of HIV provirus within the CCR2/5⁺ cells was 37% (Fig. 6D). Importantly, the CCR2/5⁺ cells had the highest proportion of integrated HIV of all the

sorted subsets. These results suggested that CCR2/5⁺ cells formed a significant fraction of the latent HIV reservoir *in vivo*.

DISCUSSION

Our findings support the notion that CCR2/5⁺ CD4 T cells found in human lymphoid tissue can act as reservoir cells during HIV infection: first, these cells are permissive to HIV infection; second, blockade of CCL2 action in infected humanized mice decreases seeding of the latent reservoir; and third, the CCR2/5⁺ CD4 T cells harbor a significant fraction of provirus that can be reactivated to seed new infections. The early production of CCL2 during HIV infection could attract these memory CD4 T cells, helping propel seeding of the latent reservoir.

Based on CRISPR-Cas9 knockout results, IFI16 and STING signaling play a role in CCL2 gene activation. However, as IFI16 and STING knockouts only partially ablate production of CCL2 in the HIV-infected CD4 T cells, CCL2 production during HIV infection likely occurs through multiple mechanisms. HIV gp120 (42–44), Tat (45–47), Nef (48), and p17 (49) have all been shown to activate CCL2. Our findings now add an additional mechanism underlying CCL2 release during HIV infection involving IFI16 sensing of abortive reverse transcription products coupled with STING signaling.

CCL2 attracts cells that express CCR2 to areas of tissue inflammation. These cells can include monocytes, CD4 T cells, and NK cells. While the circulating CCR2/5⁺ CD4 T cells in blood are predominantly effector memory cells (24), we find that CCR2/5⁺ cells in the lymphoid tissue display a central memory phenotype (Fig. 2 and 3). This pattern of chemokine receptor expression is intriguing in the context of HIV infection as it provides a potential pathogenic link between target cell recruitment (CCR2), infectibility (CCR5), and rapid establishment of a long-lived latent reservoir within central memory T cells (CCR7).

As the primary route of HIV infection is through mucosal tissues, the integrin expression profile of the CCR2/5⁺ population is particularly interesting. These cells express high surface levels of the CD49d, CD29, and $\alpha 4\beta 7$ integrins (Fig. 3) that play a key role in mucosal trafficking (50) and that are expressed on HIV-permissive cells from the female reproductive tract (51). CCR2⁺ CD4 T cells are also recruited to the ileum in inflammatory bowel disease (52). Thus, CCR2/5⁺ CD4 T cells are likely mucosal in origin or alternatively localize to mucosa or mucosa-associated lymphoid tissue (MALT). These cells may be involved in establishment of reservoirs in MALT even before migration into secondary lymphoid organs.

Our studies indicate that antibody-mediated blockade of CCL2 *in vivo* in humanized mice significantly reduces the formation of the HIV reservoir, as measured by decreased detection of plasma viremia following ART withdrawal and total detectable HIV at necropsy (Fig. 5). CCL2 blockade was administered 1 day prior to HIV exposure. We also intentionally selected a short infection period of only 6 days before initiation of ART to evaluate the establishment of the most rapidly formed stable reservoir.

Long-term effective ART contracts the population of HIV-infected cells around a core reservoir of cells infected prior to treatment. Our findings indicate that on average CCR2/5⁺ cells harbor ~35% of the reservoir when blood cells are analyzed from HIV-infected individuals on ART. However, we also noted marked differences in the fraction of the reservoir residing in CCR2/5⁺ cells among the 9 individuals analyzed (Fig. 6D). In one individual, nearly 90% of the latent reservoir was found in the CCR2/5⁺ cells. These findings suggest that CCL2 may play an important role in latent reservoir seeding in many but not all infected individuals. It is certainly possible that the underlying mechanism of infection and level of inflammation in lymphoid tissues may vary, impacting levels of CCL2 that are released and the extent to which CCR2/5⁺ chemoattraction occurs. Additionally, T cells exhibit a marked plasticity in the expression of CCR2 and other chemokine receptors (T cell stimulation and differentiation significantly modulate overall gene expression profiles [53] and cell surface proteomes [54]) which could obscure a preferential infection and initial reservoir seeding in a specific

subset of T cells. Finally, the duration of infection prior to treatment may allow for spread of the reservoir, and although CCR2⁺ cells may be initially favored, the phenotype of the reservoir likely broadens during chronic infection. CCR2-negative cells also harbored HIV provirus in all assayed individuals (Fig. 6). Therefore, CCR2 expression certainly does not perfectly mark the HIV reservoir *in vivo*, which may also include cells such as CD4⁺ Th17 cells present at portals of HIV entry.

A limitation of most reservoir studies, including this one, is that human samples are often limited to peripheral blood donated by HIV-infected individuals and therefore fail to sample the tissue reservoir. However, circulating cells of the blood originate from tissue sites. The effector memory CCR2/5⁺ cells we find containing HIV provirus are likely daughters of the initially infected lymphoid tissue-derived CCR2/5⁺ central memory cells. It is interesting that the predominant population of CCR2⁺/CCR5⁺ cells in blood corresponds to effector memory cells while the CCR2⁺/CCR5⁺ cells in lymphoid tissue exhibit properties of central memory T cells. Because the latent reservoir is predominantly found in lymphoid tissues, these findings again emphasize the importance of studying HIV interactions in lymphoid tissue-derived CD4 T cells rather than limiting studies to blood cells, which historically has been the case. The lymphoid tissue CCR2⁺/CCR5⁺ subset of cells is distinguished by elevated expression of CD25 (in the absence of FoxP3, so not Treg), CD7, ICOS, and CCR7. High-level expression of CCR7 provided a strong marker indicating their central memory phenotype. Other increased markers include CD38 and OX40, indicating a higher level of cellular activation. CD2 and CD95FasL were also increased while IFI16, a critical DNA sensor in the pyroptotic death pathway, was slightly increased in these cells. The presence of IFI16 is consistent with its role of DNA sensing during abortive infection, giving rise to CCL2 production. In contrast, blood CCR2⁺/CCR5⁺ cells were characterized by high levels of CD127 (alpha subunit of the interleukin-7 [IL-7] receptor) and CCR6, the receptor for CCL20, whereas CCR7 and CD25 were poorly expressed.

Together, our results demonstrate that lymphoid tissue CD4 T cells rapidly produce CCL2 as part of an innate inflammatory response launched during HIV infection. Among multiple mechanisms, IFI16 sensing of HIV DNA and signaling via STING contribute to rapid release of the CCL2 chemokine that can quickly recruit CCR2/5⁺ central memory cells to the zone of HIV-associated inflammation. Within these zones of infection and inflammation, some cells may become productively infected while others undergo latent infection and yet others die. Finally, we suspect the CCR2/5⁺ central memory cells ultimately take up residence in peripheral lymphoid organs harboring latent HIV provirus, contributing to the persistence of the stable reservoir. Our findings argue for a role of the CCL2/CCR2 axis in early seeding of the latent reservoir, illustrating how the innate immune response may, in this case, promote viral persistence. These results do not preclude the involvement of other pathways to persistence as recently described by Evans et al. (55).

MATERIALS AND METHODS

Experimental model and subject details. (i) Human samples. Blood from HIV-infected individuals was obtained from volunteers participating in the SCOPE cohort (56). Participants gave their informed consent as part of the SCOPE cohort. Specific characteristics of these participants and their ART regimens are summarized in Table S2 in the supplemental material.

(ii) Humanized TKO-BLT mice. Male and female C57BL/6 Rag2^{-/-} γ c^{-/-} CD47^{-/-} (TKO) mice were humanized using the bone marrow, liver, thymus (BLT) method as previously described (38). All animal studies were performed after approval of the animal study protocol by the AAALAC-accredited Rocky Mountain Laboratories, National Institute of Allergy and Infectious Diseases, National Institutes of Health (USA) Institutional Animal Care and Use Committee. The mice were housed under specific-pathogen-free conditions, properly anesthetized during procedures, and monitored daily. Donor tissues for humanization were obtained with informed consent following the guidelines and regulations of NIH and the Office of Human Subjects Research Protection. All humanized mouse studies were initiated prior to the executive order by President Trump banning government research using fetal tissue.

Humanized mice were treated intraperitoneally with 200 μ g anti-CCL2 antibody (2H5) or isotype control 24 h prior to infection followed by 100 μ g administered every 48 h for a total of 12 days. HIV-1 JR_{CSF} stocks were prepared and inoculated as previously described (55). The mice were challenged with 5×10^4 tissue culture infectious units (TCIU) of HIV via the anal route at day 0 and every 24 h for 4

additional days. At day 6 postinfection, the mice were bled retro-orbitally. At day 7, the mice were free-fed red-dyed ART-infused chow (modified LabDiet PicoLab mouse diet 20, 5058; supplemented with 1,250 ppm emtricitabine [Emtriva], 1,630 ppm tenofovir disoproxil-fumarate [Viread], and 10,688 ppm raltegravir [Isentress]) until 12 weeks postinfection, when ART was discontinued. Mice were bled at 6 weeks postinfection to test for suppression of viremia and weekly following ART interruption until the euthanasia time point at 16 weeks postinfection.

Primary cell cultures. Specimens derived from HIV-negative human blood and tissue were deidentified before receipt by the laboratory and are thus exempt from human subject research per the UCSF Human Research Protection Program Institutional Review Board. Human healthy tonsils and spleens were obtained from the Cooperative Human Tissue Network (<https://www.chtn.org>). HIV-negative donor blood was obtained from Vitalant (<https://www.vitalant.org>).

Human lymphoid aggregate culture (HLAC) prepared from tonsil or spleen was cultured in HLAC medium: RPMI supplemented with 15% heat-inactivated fetal bovine serum (FBS), 100 mg/mL gentamicin, 200 mg/mL ampicillin, 1 mM sodium pyruvate, 1% nonessential amino acids, 2 mM L-glutamine, and 1% amphotericin B (Fungizone) at 37°C in a 5% CO₂ incubator.

Concentrated white blood cell preparations from healthy volunteers were obtained from Vitalant. Peripheral blood mononuclear cells (PBMCs) were cultured in RPMI medium supplemented with 10% FBS, 1,000 U/mL penicillin, 1 mg/mL streptomycin, and 2 mM L-glutamine, at 37°C in a 5% CO₂ incubator.

Cell line. HEK293T cells were transfected with various molecular clones of HIV to produce high-titer virus preparations. Cells were cultured in Dulbecco modified Eagle medium (DMEM) supplemented with 10% FBS, 1,000 U/mL penicillin, 1 mg/mL streptomycin, and 2 mM L-glutamine, at 37°C in a 5% CO₂ incubator.

Virus strains. HIV molecular clones (pNL4-3-GFP, pBaL-GFP, and pNL4-3-Luciferase) were purified from *Escherichia coli* and used to transfect HEK293T cells. Both NL4-3-based viruses are X4-tropic, whereas pBaL-GFP is R5-tropic.

Primary cell isolation and culture. Fresh human tonsil tissue or splenic tissue was processed and cultured as previously described (57). Briefly, single-cell suspensions were prepared by mechanical disruption of the tonsil or spleen, followed by sequential passage of cells through 70- μ m and then 40- μ m strainers. Single-cell suspensions were purified by density gradient centrifugation using Ficoll-Hypaque (GE), and the mononuclear cell layer was isolated, washed twice with fluorescence-activated cell sorting (FACS) buffer, and then analyzed by flow or mass cytometry or alternatively cultured in HLAC medium. PBMCs were similarly purified by density gradient centrifugation using Ficoll-Hypaque.

CD4 T cell isolation. CD4 T cells were purified from lymphoid tissue or PBMC-derived mononuclear cells by negative magnetic depletion using the EasySep human CD4⁺ T cell enrichment kit (Stem Cell), per the manufacturer's protocol.

HIV infection (overlay model). Overlay infections were carried out as previously described (19). Briefly, HEK293T cells were seeded in 24-well tissue culture plates at a density of 1.6×10^5 cells/well and transfected with 50 to 100 ng/well of pNL4-3-GFP using Fugene HD (Promega) transfection reagent, per the manufacturer's protocol. The medium was replaced after 16 h, and CD4 T cells, purified as described above, were added. Cells or supernatants were harvested at time points indicated for each experiment.

HIV infection (spinoculation model). Concentrated HIV was produced by transfecting 5×10^6 to 10×10^6 HEK293T cells per T150 flask with pNL4-3-GFP, pBaL-GFP, or pNL4-3-Luciferase, using Fugene HD per the manufacturer's protocol. The medium was replaced 16 h after transfection, and the supernatant was harvested 48 and 72 h posttransfection. Supernatant containing viruses was passed through a 0.22- μ m filter, and virus was pelleted at $25,000 \times g$ for 2 h at 4°C. Following resuspension of the pellet in RPMI medium, the concentrated viruses were aliquoted and frozen at -80°C. Virus concentration was determined by quantitation of p24⁹⁹ as previously described (19). One hundred nanograms of virus was generally added to the cell populations cultured at 1×10^5 cells/mL in 100 μ L in 96-well round-bottom tissue culture plates. The plate was spun at $900 \times g$ for 2 h at room temperature and then cultured at 37°C in a 5% CO₂ incubator.

Analysis of cytokine expression. Quantitative reverse transcriptase PCR (RT-PCR) was used to assess cytokine mRNA expression. Cells were harvested 18 to 48 h following culture or infection as described for the various experiments, and RNA was purified using the RNeasy kit (Qiagen) per the manufacturer's protocol with inclusion of DNase treatment. Purified RNA was quantified, and cDNA was prepared using the SuperScript III First-Strand synthesis kit (Thermo Fisher). RNA, oligo(dT)₂₀, and deoxynucleoside triphosphates (dNTPs) were combined and incubated at 65°C for 5 min and then cooled to 4°C. RT buffer, MgCl₂, dithiothreitol (DTT), RNaseOUT, and SuperScript III RT were added per the manufacturer's protocol and incubated at 50°C for 50 min. The reaction was terminated by heating to 85°C for 5 min, and cDNA was stored at -20°C. Following cDNA production, quantitative PCR was carried out using TaqMan gene expression assays (Thermo Fisher; see Table S3 in the supplemental material for specific assay identifiers [IDs]) per the manufacturer's protocol. Both glyceraldehyde-3-phosphate dehydrogenase (GAPDH) and 18S mRNA were measured, and the geometric means for these housekeeping genes were used to normalize expression (delta cycle threshold) of query transcripts.

Secreted CCL2 protein was measured using the Meso Scale Discovery (MSD) platform. Supernatants from cells cultured as described above were harvested and clarified by centrifugation at $1,000 \times g$ for 10 min. Undiluted supernatant was applied to the V-Plex human MCP-1 kit (Meso Scale Discovery), and CCL2 was measured using a recombinant standard, per the manufacturer's protocol.

Cas9 RNP genomic editing. Nucleofection was performed using *in vitro*-assembled Cas9 RNP as previously described (58). Recombinant Cas9 protein derived from *Streptococcus pyogenes* engineered with two nuclear localization signals and a hemagglutinin (HA) tag on the C terminus was obtained from the QB3 Macrolab at the University of California, Berkeley. Multiple guide RNAs were tested, and two were selected for each target gene that showed high knockdown efficiency in multiple donors (see Table S3

for guide sequences). Guide RNA and *trans*-activating CRISPR RNA (tracrRNA) suspended in 10 mM Tris-HCl (pH 7.4) were mixed at a 1:1 ratio, at a final concentration of 40 μ M, and incubated for 30 min at 37°C. The guide RNA mixture was added to 40 μ M recombinant Cas9 and incubated at 37°C for 15 min to allow for assembly of the guide RNA-Cas9 RNPs.

HLAC cells were stimulated for 3 days with plates coated with 10 μ g/mL anti-CD3 (UCHT1; Tonbo Biosciences) and 10 μ g/mL anti-CD28 (CD28.2; Tonbo Biosciences). CD4 T cells were purified as described above, and 3×10^5 CD4 T cells were pelleted in a V-bottom plate and resuspended in 20 μ L P3 buffer, from the P3 Primary Cell 96-well Nucleofector kit (Lonza). Three microliters of the assembled Cas9 RNPs was added to the cells, and the mixture was transferred to a 96-well reaction cuvette. The cuvettes were loaded into the 4D-Nucleofector (Lonza) and electroporated using program EH-115. Eighty microliters of prewarmed HLAC medium was gently added to each well, and the cells were allowed to recover for 30 min at 37°C, before restimulating overnight on plates as described above. Following Cas9 RNP-mediated editing, the cells were removed from stimulation and rested for 1 week before infection or subsequent analyses. Knockout efficiencies were measured using immunoblotting or intracellular flow cytometry.

Immunoblotting. Cell lysates were prepared by addition of Laemmli lysis buffer and heat denaturation at 90°C for 30 min. Lysates were electrophoresed on a 4 to 12% Bis-Tris gel (Thermo Fisher) at 120 V for 90 min. Proteins were transferred to a polyvinylidene difluoride (PVDF) membrane using an iBlot 2 apparatus per the manufacturer's protocol (default program P1). Following transfer, the membrane was blocked with 5% (wt/vol) dry skim milk dissolved in phosphate-buffered saline (PBS) plus 0.1% Tween 20 (PBS-T) for 1 h at room temperature with rocking. Blocked membranes were incubated with primary antibodies (see Table S3), diluted in blocking buffer (1:1,000), and incubated with rocking overnight at 4°C. The following day, membranes were washed in PBS-T and incubated with horseradish peroxidase (HRP)-conjugated secondary antibody diluted 1:10,000 in blocking buffer for 2 h at room temperature with continuous rocking. After secondary incubation, the membranes were washed and tetramethylbenzidine (TMB) substrate was added. The reaction was allowed to proceed for 5 min, and light was measured by exposure to film.

Flow cytometric analysis and cell sorting. Flow cytometry was performed at the Gladstone Institutes Flow Cytometry Core Facility using two instruments: an LSR II (BD Biosciences, San Diego, CA, USA) and a FACSAria II (BD Biosciences, San Diego, CA, USA). Cells were resuspended in PBS, and Zombie Live/Dead (BioLegend) stain was added per the manufacturer's protocol. Subsequently, FACS buffer (PBS plus 2 mM EDTA plus 5% bovine serum albumin [BSA]) was added as well as antibodies for cell surface staining (see Table S3). Cells were washed and sorted live or fixed in 2% paraformaldehyde (PFA) prior to analysis. For intracellular antigen detection, cells were permeabilized after cell surface staining, using the Foxp3/transcription factor staining buffer set (Thermo Fisher) and following the manufacturer's protocol.

Fluorescence-activated cell sorting was performed on unfixed live cells, following isolation and surface staining as described above. Single cells from a lymphocyte scatter gate were gated as "live" (Zombie low/negative; see Table S3) and subsequently as CD3⁺/4⁺ T cells. CD4⁺ T cells were then sorted as naive (CD45RO⁻) or memory (CD45RO⁺) and further subdivided as CCR2⁻/5⁻, CCR2⁺/5⁻, CCR2⁻/5⁺, or CCR2⁺/5⁺ (Fig. 6 shows an example). Cells were sorted into ice-cold HLAC medium for functional studies as described above or sorted into ice-cold PBS and pelleted, and genomic DNA was isolated for HIV provirus measurements.

Mass cytometric analysis. Mass cytometric analysis was performed as previously described (59). Cells were isolated from fresh PBMCs or HLAC as described above and stained with a panel of lanthanide metal-conjugated antibodies (Table S1). Antibody staining was performed in a volume of 100 μ L for 45 min, which was treated with 139In-DOTA-maleimide (MacroCyclics) to label dead cells and fixed overnight with PBS plus 2% PFA. Cells were permeabilized with FoxP3 Fix/Perm buffer (Thermo Fisher) per the manufacturer's protocol and then labeled with 1:4,000 191/193Ir DNA intercalator (Fluidigm). Cells were washed, resuspended in distilled water, and analyzed on a CyTOF2 (Fluidigm) at the UCSF Parnassus Flow Cytometry Core. EQ calibration beads (Fluidigm) were included and used for normalization across runs.

Chemotaxis measurement. CCR2/5⁺ CD4⁺ T cells were purified by FACS and suspended at 1×10^6 cells/mL in RPMI with 0.5% BSA and 25 mM HEPES. One hundred microliters of sorted cells was added to each transwell insert with 6.5-mm-diameter membranes containing 3.0- μ m pores (Corning). The cells were preincubated for 30 min at 37°C, and the inserts were transferred into wells with chemotaxis medium containing either CCL2 (1 μ g/mL; PeproTech) or medium alone. Cells in the lower wells were harvested after 3 h at 37°C, and the migrated cells were counted using AccuCount particles on an LSR II cytometer.

In vitro latency. As previously described, purified CD4 T cells were initially infected and then rested in the presence of ART to establish *in vitro* latency (36). Briefly, tonsil-derived purified resting (unstimulated) memory CD4 T cells were sorted based on their expression of CCR2 and CCR5 as described above. One hundred nanograms of purified NL4-3-luciferase was added to the sorted cells, they were spinoculated as described above, and 5 μ M saquinavir was added to limit infection to a single round. Following 5 days of culture, the cells were stimulated with anti-CD3/CD28 beads per the manufacturer's protocol, in the presence of 30 μ M raltegravir. At 24 h after stimulation, luciferase activity was measured as previously described (36).

HIV Alu-Gag droplet digital qPCR. Nested Alu-Gag qPCR was performed as previously described (60, 61) with minor modifications. Briefly, genomic DNA was isolated using DNeasy kits using the RNase treatment step (Qiagen) per the manufacturer's protocol. A primary PCR to amplify integrated provirus

used a forward Alu-targeting primer at a concentration of 100 nM and an HIV-1 Gag reverse primer at 600 nM. Preamplification was performed with *Taq* polymerase (Qiagen) for 20 cycles. One microliter of the above PCR product was combined with 10 μ L Gene Expression master mix (Applied Biosciences), 8 μ L water, 1 μ L probe mix (premade 20 \times mix: 5 μ M MH531 and MH532 primers, 4 μ M long-terminal-repeat (LTR) probe). The PCR mixture was partitioned using a QX200 droplet generator (Bio-Rad), and the droplets were amplified (95°C for 15 s, 60°C for 30 s multiplied by 35 cycles). Positive and negative droplets were then detected on a QX200 droplet reader (Bio-Rad), and the results were quantified using QuantaSoft software.

Measurement of HIV in TKO-BLT humanized mice. Plasma HIV RNA was isolated with the QIAamp viral RNA kit (Qiagen) and quantified using the Abbott RealTime HIV-1 amplification reagent kit following the manufacturer's protocols. Depending on the available sample volume, the detection limit was 375 copies/ml (cp/mL) during follow-up or 150 cp/mL at the time of euthanasia. For the quantification of HIV DNA, genomic DNA of splenocytes was isolated using the QIAamp DNA blood minikit (Qiagen) and subjected to a probe-based real-time PCR approach, as previously described (38, 62). Briefly, HIV-specific and control (hCD3) DNA sequences were preamplified (12 cycles) in a TProfessional Trio Thermocycler (Biometra). The pre-PCR amplicons were subjected to quantitative real-time PCR analysis using the Rotor-Gene probe PCR kit (Qiagen) performed in a Rotor-Gene Q instrument (Qiagen). Dual-labeled probes were used for CD3 [Yakima Yellow (YAK)-black hole quencher 1 (BHQ1)] and HIV-DNA (6-carboxyfluorescein [FAM]-BHQ1) detection. Plasmids carrying the corresponding amplicon regions or gDNA of cells harboring HIV-long terminal repeat (LTR) sequences were used as standard curves (37, 38).

Quantification and statistical analysis. Statistical details of individual experiments, including number of independent donors, mean values, standard error of the mean (SEM), and *P* values derived from statistical tests, are described in the figure legends and specified in the figures. Statistical analyses were performed using GraphPad Prism software versions 7 and 8. *P* values of ≤ 0.05 were considered statistically significant. For two-way column analyses, a Student two-tailed *t* test was used. Analyses of variance (ANOVAs) were used for multiple comparisons with posttests for multiple comparisons (as noted within). Asterisk coding in figures is as follows: *, $P \leq 0.05$; **, $P \leq 0.01$; ***, $P \leq 0.001$. Data are presented as means with error bars indicating SEM unless otherwise stated.

Data and code availability. This study did not generate data sets.

SUPPLEMENTAL MATERIAL

Supplemental material is available online only.

FIG S1, PDF file, 0.03 MB.

FIG S2, PDF file, 0.3 MB.

FIG S3, PDF file, 0.1 MB.

FIG S4, PDF file, 0.1 MB.

FIG S5, PDF file, 0.1 MB.

TABLE S1, DOCX file, 0.04 MB.

TABLE S2, DOCX file, 0.04 MB.

TABLE S3, DOCX file, 0.05 MB.

ACKNOWLEDGMENTS

We thank Jane Srivastava and Nandhini Raman of the Gladstone Flow Cytometry Core, the UCSF Diabetes Research Center for use of their CyTOF instrument, the UCSF Parnassus Flow Cytometry Core for CyTOF assistance, John C. W. Carroll for graphic arts, Francoise Chanut for editorial assistance, and Robin Givens for administrative assistance.

Research reported in this publication was supported by the NIAID Intramural Research Program, NIAID, NHLBI, NIDA, NINDS, NIMH, and NIDDK of the National Institutes of Health under award number UM1AI164559 to the HOPE Collaboratory and R01 AI147777, R01 AI127219, and P01 AI131374. The Gladstone Institutes acknowledges the generous support of the James B. Pendleton Charitable Trust. M.W. and U.D. were supported by the DFG priority program 556 SPP1923 (WI 5086/1-1 and DI 714/18-2).

The content is solely the responsibility of the authors and does not necessarily represent the official views of the National Institutes of Health.

There are no competing interests.

REFERENCES

- Whitney JB, Hill AL, Sanisetty S, Penaloza-MacMaster P, Liu J, Shetty M, Parenteau L, Cabral C, Shields J, Blackmore S, Smith JY, Brinkman AL, Peter LE, Mathew SI, Smith KM, Borducchi EN, Rosenbloom DI, Lewis MG, Hattersley J, Li B, Hesselgesser J, Geleziunas R, Robb ML, Kim JH, Michael NL, Barouch DH. 2014. Rapid seeding of the viral reservoir prior to SIV viraemia in rhesus monkeys. *Nature* 512:74–77. <https://doi.org/10.1038/nature13594>.
- Colby DJ, Trautmann L, Pinyakorn S, Leyre L, Pagliuzza A, Kroon E, Rolland M, Takata H, Buranapraditkun S, Intasan J, Chomchey N, Muir R, Haddad EK, Tovanabutra S, Ubolyam S, Bolton DL, Fullmer BA, Gorelick RJ, Fox L, Crowell TA, Trichavaroj R, O'Connell R, Chomont N, Kim JH, Michael NL, Robb ML, Phanuphak N, Ananworanich J, RV411 study group. 2018. Rapid HIV RNA rebound after antiretroviral treatment interruption in persons

- durably suppressed in Fiebig I acute HIV infection. *Nat Med* 24:923–926. <https://doi.org/10.1038/s41591-018-0026-6>.
3. Chun TW, Engel D, Berrey MM, Shea T, Corey L, Fauci AS. 1998. Early establishment of a pool of latently infected, resting CD4(+) T cells during primary HIV-1 infection. *Proc Natl Acad Sci U S A* 95:8869–8873. <https://doi.org/10.1073/pnas.95.15.8869>.
 4. Henrich TJ, Hatano H, Bacon O, Hogan LE, Rutishauser R, Hill A, Kearney MF, Anderson EM, Buchbinder SP, Cohen SE, Abdel-Mohsen M, Pohlmeier CW, Fromentin R, Hoh R, Liu AY, McCune JM, Spindler J, Metcalf-Pate K, Hobbs KS, Thanh C, Gibson EA, Kuritzkes DR, Siliciano RF, Price RW, Richman DD, Chomont N, Siliciano JD, Mellors JW, Yu KL, Blankson JN, Liegler T, Deeks SG. 2017. HIV-1 persistence following extremely early initiation of antiretroviral therapy (ART) during acute HIV-1 infection: an observational study. *PLoS Med* 14:e1002417. <https://doi.org/10.1371/journal.pmed.1002417>.
 5. Abrahams MR, Joseph SB, Garrett N, Tyers L, Moeser M, Archin N, Council OD, Matten D, Zhou S, Doolabh D, Anthony C, Goonetilleke N, Karim SA, Margolis DM, Pond SK, Williamson C, Swanstrom R. 2019. The replication-competent HIV-1 latent reservoir is primarily established near the time of therapy initiation. *Sci Transl Med* 11:eaaw5589. <https://doi.org/10.1126/scitranslmed.aaw5589>.
 6. Brodin J, Zanini F, Thebo L, Lanz C, Bratt G, Neher RA, Albert J. 2016. Establishment and stability of the latent HIV-1 DNA reservoir. *Elife* 5:e18889. <https://doi.org/10.7554/eLife.18889>.
 7. Jones BR, Kinloch NN, Horacek J, Ganase B, Harris M, Harrigan PR, Jones RB, Brockman MA, Joy JB, Poon AFY, Brumme ZL. 2018. Phylogenetic approach to recover integration dates of latent HIV sequences within-host. *Proc Natl Acad Sci U S A* 115:E8958–E8967. <https://doi.org/10.1073/pnas.1802028115>.
 8. Klatt NR, Chomont N, Douek DC, Deeks SG. 2013. Immune activation and HIV persistence: implications for curative approaches to HIV infection. *Immunol Rev* 254:326–342. <https://doi.org/10.1111/immr.12065>.
 9. Ochsenbauer C, Edmonds TG, Ding H, Keele BF, Decker J, Salazar MG, Salazar-Gonzalez JF, Shattock R, Haynes BF, Shaw GM, Hahn BH, Kappes JC. 2012. Generation of transmitted/founder HIV-1 infectious molecular clones and characterization of their replication capacity in CD4 T lymphocytes and monocyte-derived macrophages. *J Virol* 86:2715–2728. <https://doi.org/10.1128/JVI.06157-11>.
 10. Parker ZF, Iyer SS, Wilen CB, Parrish NF, Chikere KC, Lee FH, Didigu CA, Berro R, Klasse PJ, Lee B, Moore JP, Shaw GM, Hahn BH, Doms RW. 2013. Transmitted/founder and chronic HIV-1 envelope proteins are distinguished by differential utilization of CCR5. *J Virol* 87:2401–2411. <https://doi.org/10.1128/JVI.02964-12>.
 11. Chomont N, El-Far M, Ancuta P, Trautmann L, Procopio FA, Yassine-Diab B, Boucher G, Boulassel MR, Ghattas G, Brenchley JM, Schacker TW, Hill BJ, Douek DC, Routy JP, Haddad EK, Sekaly RP. 2009. HIV reservoir size and persistence are driven by T cell survival and homeostatic proliferation. *Nat Med* 15:893–900. <https://doi.org/10.1038/nm.1972>.
 12. Siliciano JM, Siliciano RF. 2015. The remarkable stability of the latent reservoir for HIV-1 in resting memory CD4+ T cells. *J Infect Dis* 212:1345–1347. <https://doi.org/10.1093/infdis/jiv219>.
 13. Murray AJ, Kwon KJ, Farber DL, Siliciano RF. 2016. The latent reservoir for HIV-1: how immunologic memory and clonal expansion contribute to HIV-1 persistence. *J Immunol* 197:407–417. <https://doi.org/10.4049/jimmunol.1600343>.
 14. Estes JD, Kityo C, Ssali F, Swainson L, Makamdop KN, Del Prete GQ, Deeks SG, Luciw PA, Chipman JG, Beilman GJ, Hoskuldsson T, Khoruts A, Anderson J, Deleage C, Jasurda J, Schmidt TE, Hafertepe M, Callisto SP, Pearson H, Reimann T, Schuster J, Schoephoerster J, Southern P, Perkey K, Shang L, Wietgreffe SW, Fletcher CV, Lifson JD, Douek DC, McCune JM, Haase AT, Schacker TW. 2017. Defining total-body AIDS-virus burden with implications for curative strategies. *Nat Med* 23:1271–1276. <https://doi.org/10.1038/nm.4411>.
 15. Weiss L, Si-Mohamed A, Giral P, Castiel P, Ledur A, Blondin C, Kazatchkine MD, Haeflner-Cavaillon N. 1997. Plasma levels of monocyte chemoattractant protein-1 but not those of macrophage inhibitory protein-1alpha and RANTES correlate with virus load in human immunodeficiency virus infection. *J Infect Dis* 176:1621–1624. <https://doi.org/10.1086/517341>.
 16. Ansari AW, Bhatnagar N, Dittrich-Breiholz O, Kracht M, Schmidt RE, Heiken H. 2006. Host chemokine (C-C motif) ligand-2 (CCL2) is differentially regulated in HIV type 1 (HIV-1)-infected individuals. *Int Immunol* 18:1443–1451. <https://doi.org/10.1093/intimm/dx1078>.
 17. Covino DA, Sabbatucci M, Fantuzzi L. 2016. The CCL2/CCR2 axis in the pathogenesis of HIV-1 infection: a new cellular target for therapy? *Curr Drug Targets* 17:76–110. <https://doi.org/10.2174/138945011701151217110917>.
 18. Stacey AR, Norris PJ, Qin L, Haygreen EA, Taylor E, Heitman J, Lebedeva M, DeCamp A, Li D, Grove D, Self SG, Borrow P. 2009. Induction of a striking systemic cytokine cascade prior to peak viremia in acute human immunodeficiency virus type 1 infection, in contrast to more modest and delayed responses in acute hepatitis B and C virus infections. *J Virol* 83:3719–3733. <https://doi.org/10.1128/JVI.01844-08>.
 19. Munoz-Arias I, Doitsh G, Yang Z, Sowinski S, Ruelas D, Greene WC. 2015. Blood-derived CD4 T cells naturally resist pyroptosis during abortive HIV-1 infection. *Cell Host Microbe* 18:463–470. <https://doi.org/10.1016/j.chom.2015.09.010>.
 20. Sanchez DJ, Miranda D, Jr, Marsden MD, Dizon TM, Bontemps JR, Davila SJ, Del Mundo LE, Ha T, Senaati A, Zack JA, Cheng G. 2015. Disruption of type I interferon induction by HIV infection of T cells. *PLoS One* 10:e0137951. <https://doi.org/10.1371/journal.pone.0137951>.
 21. Galloway NL, Doitsh G, Monroe KM, Yang Z, Munoz-Arias I, Levy DN, Greene WC. 2015. Cell-to-cell transmission of HIV-1 is required to trigger pyroptotic death of lymphoid-tissue-derived CD4 T cells. *Cell Rep* 12:1555–1563. <https://doi.org/10.1016/j.celrep.2015.08.011>.
 22. Matsushima K, Larsen CG, DuBois GC, Oppenheim JJ. 1989. Purification and characterization of a novel monocyte chemotactic and activating factor produced by a human myelomonocytic cell line. *J Exp Med* 169:1485–1490. <https://doi.org/10.1084/jem.169.4.1485>.
 23. Deshmane SL, Kremlev S, Amini S, Sawaya BE. 2009. Monocyte chemoattractant protein-1 (MCP-1): an overview. *J Interferon Cytokine Res* 29:313–326. <https://doi.org/10.1089/jir.2008.0027>.
 24. Zhang HH, Song K, Rabin RL, Hill BJ, Perfetto SP, Roederer M, Douek DC, Siegel RM, Farber JM. 2010. CCR2 identifies a stable population of human effector memory CD4+ T cells equipped for rapid recall response. *J Immunol* 185:6646–6663. <https://doi.org/10.4049/jimmunol.0904156>.
 25. Sallusto F, Geginat J, Lanzavecchia A. 2004. Central memory and effector memory T cell subsets: function, generation, and maintenance. *Annu Rev Immunol* 22:745–763. <https://doi.org/10.1146/annurev.immunol.22.012703.104702>.
 26. Murray JM, Zaunders JJ, McBride KL, Xu Y, Bailey M, Suzuki K, Cooper DA, Emery S, Kelleher AD, Koelsch KK, PINT Study Team. 2014. HIV DNA subspecies persist in both activated and resting memory CD4+ T cells during antiretroviral therapy. *J Virol* 88:3516–3526. <https://doi.org/10.1128/JVI.03331-13>.
 27. Chachage M, Pollakis G, Kuffour EO, Haase K, Bauer A, Nadai Y, Podola L, Clowes P, Schiemann M, Henkel L, Hoffmann D, Joseph S, Bhujji S, Maboko L, Sarfo FS, Eberhardt K, Hoelscher M, Feldt T, Saathoff E, Geldmacher C. 2016. CD25+ FoxP3+ memory CD4 T cells are frequent targets of HIV infection in vivo. *J Virol* 90:8954–8967. <https://doi.org/10.1128/JVI.00612-16>.
 28. Fromentin R, Bakeman W, Lawani MB, Khoury G, Hartogensis W, DaFonseca S, Killian M, Epling L, Hoh R, Sinclair E, Hecht FM, Bacchetti P, Deeks SG, Lewin SR, Sekaly RP, Chomont N. 2016. CD4+ T cells expressing PD-1, TIGIT and LAG-3 contribute to HIV persistence during ART. *PLoS Pathog* 12:e1005761. <https://doi.org/10.1371/journal.ppat.1005761>.
 29. Kuo HH, Ahmad R, Lee GQ, Gao C, Chen HR, Ouyang Z, Szucs MJ, Kim D, Tsibris A, Chun TW, Battivelli E, Verdin E, Rosenberg ES, Carr SA, Yu XG, Lichterfeld M. 2018. Anti-apoptotic protein BIRC5 maintains survival of HIV-1-infected CD4(+) T cells. *Immunity* 48:1183–1194.e5. <https://doi.org/10.1016/j.immuni.2018.04.004>.
 30. Neidleman J, Luo X, McGregor M, Xie G, Murray V, Greene WC, Lee SA, Roan NR. 2021. mRNA vaccine-induced T cells respond identically to SARS-CoV-2 variants of concern but differ in longevity and homing properties depending on prior infection status. *bioRxiv*. <https://doi.org/10.1101/2021.05.12.443888>.
 31. Jolly C, Mitar I, Sattentau QJ. 2007. Adhesion molecule interactions facilitate human immunodeficiency virus type 1-induced virological synapse formation between T cells. *J Virol* 81:13916–13921. <https://doi.org/10.1128/JVI.01585-07>.
 32. Berlin C, Berg EL, Briskin MJ, Andrew DP, Kilshaw PJ, Holzmann B, Weissman IL, Hamann A, Butcher EC. 1993. Alpha 4 beta 7 integrin mediates lymphocyte binding to the mucosal vascular addressin MAdCAM-1. *Cell* 74:185–195. [https://doi.org/10.1016/0092-8674\(93\)90305-A](https://doi.org/10.1016/0092-8674(93)90305-A).
 33. Davila SJ, Olive AJ, Starnbach MN. 2014. Integrin alpha4beta1 is necessary for CD4+ T cell-mediated protection against genital Chlamydia trachomatis infection. *J Immunol* 192:4284–4293. <https://doi.org/10.4049/jimmunol.1303238>.
 34. Campbell GR, Spector SA. 2008. CCL2 increases X4-tropic HIV-1 entry into resting CD4+ T cells. *J Biol Chem* 283:30745–30753. <https://doi.org/10.1074/jbc.M804112200>.
 35. Hsiao F, Frouard J, Gramatica A, Xie G, Telwatte S, Lee GQ, Roychoudhury P, Schwarzer R, Luo X, Yukl SA, Lee S, Hoh R, Deeks SG, Jones RB, Cavois M, Greene WC, Roan NR. 2020. Tissue memory CD4+ T cells expressing IL-7 receptor-alpha (CD127) preferentially support latent HIV-1 infection. *PLoS Pathog* 16:e1008450. <https://doi.org/10.1371/journal.ppat.1008450>.

36. Lassen KG, Hebbeler AM, Bhattacharyya D, Lobritz MA, Greene WC. 2012. A flexible model of HIV-1 latency permitting evaluation of many primary CD4 T-cell reservoirs. *PLoS One* 7:e30176. <https://doi.org/10.1371/journal.pone.0030176>.
37. Widera M, Dirks M, Bleekmann B, Jablonka R, Daumer M, Walter H, Ehret R, Verheyen J, Esser S. 2017. HIV-1 persistent viremia is frequently followed by episodes of low-level viremia. *Med Microbiol Immunol* 206: 203–215. <https://doi.org/10.1007/s00430-017-0494-1>.
38. Lavender KJ, Pace C, Sutter K, Messer RJ, Pouncey DL, Cummins NW, Natesampillai S, Zheng J, Goldsmith J, Widera M, Van Dis ES, Phillips K, Race B, Dittmer U, Kukulj G, Hasenkrug KJ. 2018. An advanced BLT-humanized mouse model for extended HIV-1 cure studies. *AIDS* 32:1–10. <https://doi.org/10.1097/QAD.0000000000001674>.
39. Lavender KJ, Pang WW, Messer RJ, Duley AK, Race B, Phillips K, Scott D, Peterson KE, Chan CK, Dittmer U, Dudek T, Allen TM, Weissman IL, Hasenkrug KJ. 2013. BLT-humanized C57BL/6 Rag2^{-/-}gammac^{-/-}CD47^{-/-} mice are resistant to GVHD and develop B- and T-cell immunity to HIV infection. *Blood* 122: 4013–4020. <https://doi.org/10.1182/blood-2013-06-506949>.
40. Sutter K, Lavender KJ, Messer RJ, Widera M, Williams K, Race B, Hasenkrug KJ, Dittmer U. 2019. Concurrent administration of IFNalpha14 and cART in TKO-BLT mice enhances suppression of HIV-1 viremia but does not eliminate the latent reservoir. *Sci Rep* 9:18089. <https://doi.org/10.1038/s41598-019-54650-9>.
41. Mexas AM, Graf EH, Pace MJ, Yu JJ, Papasavvas E, Azzoni L, Busch MP, Di Mascio M, Foulkes AS, Migueles SA, Montaner LJ, O'Doherty U. 2012. Concurrent measures of total and integrated HIV DNA monitor reservoirs and ongoing replication in eradication trials. *AIDS* 26:2295–2306. <https://doi.org/10.1097/QAD.0b013e32835a5c2f>.
42. Bruno R, Galastri S, Sacchi P, Cima S, Caligiuri A, DeFranco R, Milani S, Gessani S, Fantuzzi L, Liotta F, Frosali F, Antonucci G, Pinzani M, Marra F. 2010. gp120 modulates the biology of human hepatic stellate cells: a link between HIV infection and liver fibrogenesis. *Gut* 59:513–520. <https://doi.org/10.1136/gut.2008.163287>.
43. Del Corno M, Gauzzi MC, Penna G, Belardelli F, Adorini L, Gessani S. 2005. Human immunodeficiency virus type 1 gp120 and other activation stimuli are highly effective in triggering alpha interferon and CC chemokine production in circulating plasmacytoid but not myeloid dendritic cells. *J Virol* 79:12597–12601. <https://doi.org/10.1128/JVI.79.19.12597-12601.2005>.
44. Kapasi A, Bhat P, Singhal PC. 1998. Tubular cell and HIV-1 gp120 interaction products promote migration of monocytes. *Inflammation* 22:137–144. <https://doi.org/10.1023/A:1022331905200>.
45. Conant K, Garzino-Demo A, Nath A, McArthur JC, Halliday W, Power C, Gallo RC, Major EO. 1998. Induction of monocyte chemoattractant protein-1 in HIV-1 Tat-stimulated astrocytes and elevation in AIDS dementia. *Proc Natl Acad Sci U S A* 95:3117–3121. <https://doi.org/10.1073/pnas.95.6.3117>.
46. Huang W, Rha GB, Han MJ, Eum SY, Andras IE, Zhong Y, Hennig B, Toborek M. 2008. PPARalpha and PPARgamma effectively protect against HIV-induced inflammatory responses in brain endothelial cells. *J Neurochem* 107:497–509. <https://doi.org/10.1111/j.1471-4159.2008.05626.x>.
47. Weiss JM, Nath A, Major EO, Beran JW. 1999. HIV-1 Tat induces monocyte chemoattractant protein-1-mediated monocyte transmigration across a model of the human blood-brain barrier and up-regulates CCR5 expression on human monocytes. *J Immunol* 163:2953–2959.
48. Lehmann MH, Masanetz S, Kramer S, Erfle V. 2006. HIV-1 Nef upregulates CCL2/MCP-1 expression in astrocytes in a myristoylation- and calmodulin-dependent manner. *J Cell Sci* 119:4520–4530. <https://doi.org/10.1242/jcs.03231>.
49. Marini E, Tiberio L, Caracciolo S, Tosti G, Guzman CA, Schiaffonati L, Fiorentini S, Caruso A. 2008. HIV-1 matrix protein p17 binds to monocytes and selectively stimulates MCP-1 secretion: role of transcriptional factor AP-1. *Cell Microbiol* 10:655–666. <https://doi.org/10.1111/j.1462-5822.2007.01073.x>.
50. Denucci CC, Mitchell JS, Shimizu Y. 2009. Integrin function in T-cell homing to lymphoid and nonlymphoid sites: getting there and staying there. *Crit Rev Immunol* 29:87–109. <https://doi.org/10.1615/critrevimmunol.v29.i2.10>.
51. Ma T, Luo X, George AF, Mukherjee G, Sen N, Spitzer TL, Giudice LC, Greene WC, Roan NR. 2020. HIV efficiently infects T cells from the endometrium and remodels them to promote systemic viral spread. *Elife* 9: e55487. <https://doi.org/10.7554/eLife.55487>.
52. Connor SJ, Paraskevopoulos N, Newman R, Cuan N, Hampartzoumian T, Lloyd AR, Grimm MC. 2004. CCR2 expressing CD4+ T lymphocytes are preferentially recruited to the ileum in Crohn's disease. *Gut* 53:1287–1294. <https://doi.org/10.1136/gut.2003.028225>.
53. Lee MS, Hanspers K, Barker CS, Korn AP, McCune JM. 2004. Gene expression profiles during human CD4+ T cell differentiation. *Int Immunol* 16: 1109–1124. <https://doi.org/10.1093/intimm/dxh112>.
54. Graessel A, Hauck SM, von Toerne C, Kloppmann E, Goldberg T, Koppensteiner H, Schindler M, Knapp B, Krause L, Dietz K, Schmidt-Weber CB, Suttner K. 2015. A combined omics approach to generate the surface atlas of human naive CD4+ T cells during early T-cell receptor activation. *Mol Cell Proteomics* 14: 2085–2102. <https://doi.org/10.1074/mcp.M114.045690>.
55. Evans VA, Khoury G, Saleh S, Cameron PU, Lewin SR. 2012. HIV persistence: chemokines and their signalling pathways. *Cytokine Growth Factor Rev* 23:151–157. <https://doi.org/10.1016/j.cytogfr.2012.05.002>.
56. Hunt PW, Martin JN, Sinclair E, Bredt B, Hagos E, Lampiris H, Deeks SG. 2003. T cell activation is associated with lower CD4+ T cell gains in human immunodeficiency virus-infected patients with sustained viral suppression during antiretroviral therapy. *J Infect Dis* 187:1534–1543. <https://doi.org/10.1086/374786>.
57. Doitsh G, Cavrois M, Lassen KG, Zepeda O, Yang Z, Santiago ML, Hebbeler AM, Greene WC. 2010. Abortive HIV infection mediates CD4 T cell depletion and inflammation in human lymphoid tissue. *Cell* 143:789–801. <https://doi.org/10.1016/j.cell.2010.11.001>.
58. Hultquist JF, Schumann K, Woo JM, Manganaro L, McGregor MJ, Doudna J, Simon V, Krogan NJ, Marson A. 2016. A Cas9 ribonucleoprotein platform for functional genetic studies of HIV-host interactions in primary human T cells. *Cell Rep* 17:1438–1452. <https://doi.org/10.1016/j.celrep.2016.09.080>.
59. Cavrois M, Banerjee T, Mukherjee G, Raman N, Hussien R, Rodriguez BA, Vasquez J, Spitzer MH, Lazarus NH, Jones JJ, Ochsenbauer C, McCune JM, Butcher EC, Arvin AM, Sen N, Greene WC, Roan NR. 2017. Mass cytometric analysis of HIV entry, replication, and remodeling in tissue CD4+ T cells. *Cell Rep* 20:984–998. <https://doi.org/10.1016/j.celrep.2017.06.087>.
60. Butler SL, Hansen MS, Bushman FD. 2001. A quantitative assay for HIV DNA integration in vivo. *Nat Med* 7:631–634. <https://doi.org/10.1038/87979>.
61. O'Doherty U, Swiggard WJ, Jeyakumar D, McGain D, Malim MH. 2002. A sensitive, quantitative assay for human immunodeficiency virus type 1 integration. *J Virol* 76:10942–10950. <https://doi.org/10.1128/jvi.76.21.10942-10950.2002>.
62. Vandergeeten C, Fromentin R, Merlini E, Lawani MB, DaFonseca S, Bakeman W, McNulty A, Ramgopal M, Michael N, Kim JH, Ananworanich J, Chomont N. 2014. Cross-clade ultrasensitive PCR-based assays to measure HIV persistence in large-cohort studies. *J Virol* 88:12385–12396. <https://doi.org/10.1128/JVI.00609-14>.